Journal of Information Systems Engineering and Management
2025, 10(47s)
e-ISSN: 2468-4376
https://www.jisem-journal.com/

Research Article

Metaheuristic Optimization of PID Controllers for Improved Stability and Oscillation Control in Solar PV and Battery-Integrated DC

Muhamad Nabil Bin Hidayat[1], Naeem Hannoon*[2], Wan Noraishah Wan Abdul Munim[3], Rahimi Baharom[4]
[1,2,4]*School of Electrical Engineering, College of Engineering, Universiti Teknologi Mara, Shah Alam, Malaysia.*
[3]*Department of EEE, ITER, SOA Deemed to be University, Odisha, India*

ARTICLE INFO

Received: 18 Dec 2024

Revised: 10 Feb 2025

Accepted: 28 Feb 2025

ABSTRACT

A DC microgrid is increasingly preferred for integrating renewable energy sources such as solar, wind, and biodiesel for electrical power distribution. Solar photovoltaic (PV) power generation, in particular, is often supported by a battery energy storage system (BESS) to ensure continuous and reliable power supply to the loads. To maximize power extraction from solar or wind sources, Maximum Power Point Tracking (MPPT) combined with DC-to-DC voltage control plays a crucial role. This paper analyzes the early synchronization and MPPT of solar power with the grid, as well as the enhanced active power transfer capability. For this purpose, Metaheuristic Optimization-based Proportional Integral and Derivative (MOPID) controllers, such as Whale Optimization Algorithm (WOA) and Grey-Wolf Optimization (GWO), are compared to demonstrate their operational effectiveness. These controllers are incorporated into the control scheme of the solar MPPT DC-DC converter, offering improved damping, better power transfer capability, faster settling times, and reduced overshoot compared to systems without controllers. The performance of the system is verified using MATLAB/Simulink in a simple DC-microgrid environment.

Keywords: Solar photovoltaic (P.V.), Microgrid (M.G.), Power Oscillations Damping, (BESS), Adaptive Fuzzy Proportional Integral and Derivative (FPID) Controller.

INTRODUCTION

With the rapid advancements in power electronics and renewable energy resources, the interest in solar photovoltaic (P.V.) cells has been growing at an exceptional rate [1]. These solar P.V. cells are being used in both developing and developed countries, with applications ranging from low-power systems, such as toys, electronic boards, lighting, and traffic control systems, to larger-scale systems for electric vehicle charging and power generation for nearby industrial loads, ranging from a few watts to several megawatts [2]. Since P.V. cells generate DC power and grids and loads typically operate on AC, at least one stage of conversion is required [3]. For handling higher power and ensuring rapid control, multi-stage converters have been widely used for years [4-6]. Recently, single-stage solar P.V. inverter topologies have gained popularity, especially for low-power, direct grid-tied applications or smaller load systems.

There has been considerable interest globally in the integration of renewable energy sources, particularly solar and wind-based power generation. According to global statistics from the wind energy organization, China, the U.S., and India are the top three countries that have each produced over 10,000 MW of solar power as of March 2018 [7]. China's solar power capacity grew from 43.5 GW in 2015 to 175 GW in 2018, with a growth rate of 3%. Other countries, such as Germany, Italy, Japan, and India, have also experienced significant growth rates, with India alone targeting 175 GW by 2022. Many countries are now allocating about 2.5% of their total budget towards renewable energy, with half of that earmarked for solar energy. In 2016, European countries had installed 98.8 GW of solar capacity, Asia 92.3 GW, East Asia 79.5 GW, North America 29.8 GW, and the remaining continents around 50 GW, totaling 323.73 GW globally. India alone produced 9,200 MW of solar power in 2017 and is progressing toward 9,600 MW for the same year.

Journal of Information Systems Engineering and Management
2025, 10(47s)
e-ISSN: 2468-4376
https://www.jisem-journal.com/

Research Article

The integration of solar P.V. systems into DC microgrids is a growing area of research. For example, the use of particle Swarm Optimization (PSO) and Perturb & Observe (P&O) algorithms for Maximum Power Point Tracking (MPPT) has been demonstrated to improve stability and dynamic response in real-time environments [9]. Additionally, fuzzy logic controllers (FLC) have been implemented in solar PV systems with DC microgrids to enhance efficiency [10]. FLC-based MPPT algorithms have been shown to be significantly faster than other control

methods, efficiency [10]. FLC-based MPPT algorithms have been shown to be significantly faster than other control methods, including neural networks and PSO [11]. Further studies have focused on improving the performance of Battery Energy Storage Systems (BESS) in solar PV systems, addressing issues like voltage variations and oscillations due to irregular irradiance and transient load conditions [12]. Additionally, various control strategies, such as dual-loop PI-based control, have been proposed to enhance the efficiency of solar PV and BESS in low-voltage DC microgrids [13].

Several metaheuristic optimization algorithms, including the Real Coded Genetic Algorithm and Artificial Neural Network-based global optimization, have been employed to enhance the performance of MPPT and fault detection in solar PV systems [14-15]. Among these, the Grey-Wolf Optimization (GWO) and Whale Optimization Algorithm (WOA) have gained attention for their ability to optimize controllers for better synchronization and active power extraction in solar PV systems. Studies have shown that hybrid methods such as PSO-GSA can improve efficiency, though they can be more complex to implement [18]. Other optimization techniques, including the Water Cycle Algorithm and Moth-Flame metaheuristic algorithms, have been explored for their applications in solving economic load dispatch and emission problems in solar PV systems [19].

Passivity-based voltage regulation methods have been applied to battery-supported solar PV systems in DC microgrids to improve transient response and stability [20, 21]. Topologies involving SEPIC converters, wind PMSG rectifiers, and bidirectional BES systems have been employed to manage load in DC microgrids [22]. Hybrid energy storage systems and distributed energy resources (DERs) have also been studied in hardware-in-loop setups to evaluate power management strategies [23]. Experimental evaluations of solar PV, batteries, and fuel cells for DC microgrid power management have been conducted [24].

Despite the significant advancements, challenges still exist in optimizing the performance of solar PV inverters, including limited power handling capabilities, varying power output characteristics, and constrained operational ranges. To overcome these challenges, researchers are working towards simpler MPPT designs with fewer switches, improved efficiency, and reduced weight, especially for rooftop installations and hybrid electric vehicle applications.
This paper focuses on comparing Grey-Wolf Optimization (GWO) and Whale Optimization Algorithm (WOA) for optimizing PID controllers in solar PV-based DC microgrids. The study aims to analyze the synchronization and active power extraction capabilities of these controllers. Key parameters such as solar PV voltage, current, micro-turbine synchronous generator, and BESS performance are verified. The goal is to ensure that the DC-DC chopper-based solar PV system achieves the following key features:

Effective operation at the Maximum Power Point Tracking (MPPT) of the P.V. cells. Capability to operate efficiently over the entire MPPT range of the P.V. array. Matching the power rating to the maximum rating of the P.V. cells. Handling the highest voltage and current ratings of the P.V. cells despite environmental temperature variations. Achieving a better performance-to-cost ratio for residential rooftop installations.

Enhanced reliability comparable to that of conventional P.V. panels. Improved efficiency. However, challenges remain, such as: Limited power handling capability. Significant variability in power output. Operational range constraints due to the imposed DC source. Increased inverter costs with higher power handling. High peak current stress with higher power handling.

Limited applicability of some MPPT techniques due to the absence of an intermediate chopper circuit.

This paper seeks to address these challenges by exploring a simpler and more efficient MPPT chopper design with

Journal of Information Systems Engineering and Management
2025, 10(47s)
e-ISSN: 2468-4376
https://www.jisem-journal.com/

Research Article

fewer switches, reduced weight, and enhanced performance compared to standard microgrid connections.

Section 2 presents the solar PV grid-tied test-bed system. Section 3 discusses the two-area solar PV test-bed system. Section 4 provides an overview of metaheuristic algorithms, including WAO and GWO, and their pseudo-codes. Section 5 presents the simulation results using GWO and WAO in the MATLAB environment. The paper concludes in Section 6, with the appendix and references provided at the end.

D.C. MICROGRID CONNECTED SOLAR P.V.BATTERY ENERGY STORAGE SYSTEM

This section presents the analytical modeling of a solar photovoltaic (P.V.) panel integrated with a Battery Energy Storage System (BESS), both connected to a common DC microgrid (M.G.) and a DC load. A detailed mathematical representation of the block diagram for the DC M.G. solar P.V. system is also provided. The modeling includes key subsystem components, switching operations, and dynamic equations for current and voltage behavior. Additionally, the output voltage equation governed by a Proportional-Integral (P.I.) controller is derived. The block diagram illustrates the interaction between the P.I. controller, the solar P.V. cell with a Maximum Power Point Tracking (MPPT) controller, and the buck-boost converter, all of which are modeled using transfer function techniques.

Modeling of Dc Microgrid based Solar PV Bess System

In general, a solar photovoltaic (P.V.) electrical power generation system is supported with a battery energy storage system (BESS) for continuous and reliability of the power supply. This solar P.V. system is connected to ac or dc or hybrid AC/DC MG. A solar P.V. dc M.G. system topology along with dc load is shown in Fig.1. This topology consists of subsystems like solar P.V. panel, solar MPPT boost converter, battery bank, bi-directional dc to dc converter connected to a common dc link terminal, buck converter for load connection. The solar P.V. panel consists of a current source with series and parallel resistances forming layers in the cell panel. This cell produces constant current and variable voltage depending on irradiation, temperature, shading, and other input factors. To extract continuous voltage from the solar P.V. cell with consistent D.C. output, the maximum power point tracking (MPPT) technique with dc voltage stepping up and to extract maximum power from the solar panel subsystem is beneficial [20-24]. The input voltage is V1, and current i1 is given to the solar MPPT cell and is boosted using a designed inductor, switch, and a diode.

The switch S1 is having a duty cycle of d1, the current through the MPPT diode D3 is i2, and the output voltage of V2 from the MPPT subsystem produces constant voltage if input parameters are stable. This voltage is equal to the dc M.G. voltage. A battery bank (BESS) with voltage E and internal resistance is in the figure supporting energy storage and retrieving when solar P.V. cells cannot supply power to the M.G. and the load. The BESS is connected to the dc M.G. using a bidirectional dc to dc converter with two switches numbered S3 and S4 with duty cycle d2. If solar power output is sufficient, the battery gets charged, else it will supply power by discharging it based on the load and grid requirement. The output from the dc M.G. is connected to the load using a buck step-down converter with the operation supported by switch S2 with duty cycle d3, inductor L3, and diode D4. The output from the buck load converter is V3 which is the voltage across the capacitor C2 and is supplied to the load R.L. The voltages and currents dynamic equations are represented.

Journal of Information Systems Engineering and Management
2025, 10(47s)
e-ISSN: 2468-4376
https://www.jisem-journal.com/

Research Article

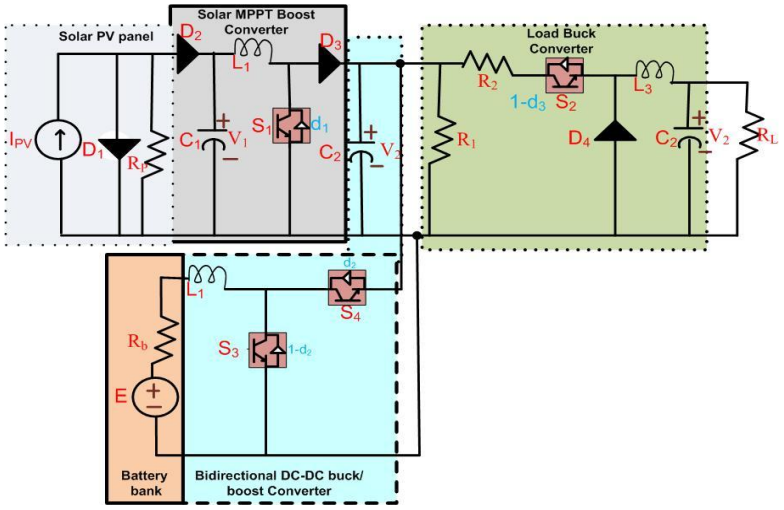

Figure 1. Solar PV BESS system connected to a dc microgrid

The input solar PV dynamic current flow is given by the equation (1)

$$L_1 \frac{di_1}{dt} = V_1 - V_2(1-d_1) \tag{1}$$

Kirchoff's current and voltage equations are used for deriving each subsystem's voltage and current. Here, V1 is solar P.V. voltage, and V2 is M.G. voltage with duty cycle d1 at switch S1 at solar MPPT boost converter [20, 21]. The battery energy storage system (BESS) dynamic current flow is given by equation (2). Here, the battery voltage is E, BESS current i2 with internal battery resistance Rb and the switch S3 at the bidirectional dc-dc buck-boost charging controller converter with duty cycle d2.

$$L_2 \frac{di_2}{dt} = E - i_2 R_b - V_2 d_2 \tag{2}$$

The load current i3 flows through the load resistance R.L. and switching operation controlling the buck voltage using the switch S2 with duty cycle d3, and the load voltage V3 is represented by the equation (3).

$$L_3 \frac{di_3}{dt} = (V_2 - i_3(1-d_3)R_L)(1-d_3) - V_3 \tag{3}$$

The solar P.V. cell output capacitor C1 dynamic voltage equation V1 is represented (4). This voltage is the difference between the source P.V. current and the boost converter current i1. The solar P.V. current iPV, diode current iD. The diode voltage constant is 'a'.

$$C_1 \frac{dV_1}{dt} = i_s - i_1 = i_{pv} - i_D(e^{aV1} - 1) - \frac{V_1}{R_p} - i_1 \tag{4}$$

The M.G. voltage dynamic equation is given by all the switches duty cycles, and the M.G. voltage is provided by the equation (5). Based on controlling the IGBT switches, voltage buck or boost operation is done, or in other terms, the dc M.G. voltage is controlled using the switches duty cycles d1, d2 and d3.

$$C_2 \frac{dV_2}{dt} = i_1(1-d_1) + i_2 d_2 - i_3(1-d_3) - \frac{V_2}{R_1} \tag{5}$$

The dc M.G. dynamic load voltage V3 equation is represented using the equation (6).

Journal of Information Systems Engineering and Management
2025, 10(47s)
e-ISSN: 2468-4376
https://www.jisem-journal.com/

Research Article

$$C_3 \frac{dV_3}{dt} = i_3 - \frac{V_3}{R_2} \quad (6)$$

The solar P.V. output regulated voltage capacitor C1 value based on a common base capacitance value is given by equation (7). Here, the P.V. capacitor voltage value is taken one-fifth times its base value-based.

$$C_1 = \frac{0.01}{0.05C_b} \quad (7)$$

If the filter capacitor, power factor variation of the M.G. is tacit within the limits of 5%. The maximum ripple current in the inductor L1 with switching time constant Tsw is given by the equation (8)

$$\Delta I_{L1\max} = \frac{2V_{dc}}{3L_1}(1-d_1)d_1T_{sw} \quad (8)$$

The same inductor ripple current represented in terms of switching frequency Fsw instead of switching time constant is shown in equation (9) and if the PV IGBT switch d1 is considered as 0.5.

$$\Delta I_{L1\max} = \frac{V_{dc}}{6F_{sw}L_1} \quad (9)$$

To obtain the maximum ripple from the panel MPPT output, if 10% ripple of rated current is considered, then the maximum ripple current is given by the equation (10),

$$\Delta I_{L1\max} = 0.1I_{\max} \quad (10)$$

Further, the maximum current output from the solar P.V. panel is given by the equation (11) represented in the form of solar P.V. real power PPV and solar P.V. input voltage V.P.V. (which is also equal to V1)

$$I_{\max} = \frac{\sqrt{2}P_{pv}}{3V_{pv}} \quad (11)$$

To reduce the current ripple to 20% with an attenuation factor Ka, the inductor MPPT L1 and battery-MG inductor L2values can be represented using the equations (12) and (13)

$$L_1 = \frac{V_{dc}}{6F_{sw}\Delta I_{L1\max}} \quad (12)$$

$$L_2 = \frac{1+\frac{1}{\sqrt{K_a^2}}}{C_2\omega_{sw}^2} \quad (13)$$

To prevent the resonant conditions, R1 and R2 are helpful.They are also responsible for the reduction of ripple on switching frequency. Hence, the resistor R1 can be represented in terms of angular resonance frequency (ωres, rad/sec) is shown in equation (14)

$$R_1 = \frac{1}{3C_2\omega_{res}} \quad (14)$$

Where the angular resonance frequency(ω_{res}) is given by the equation (15)

$$\omega_{res} = \sqrt{\frac{L_1+L_2}{L_1L_2C_2}} \quad (15)$$

The final bus voltage is given by vectorially all the subsystems voltages given by the equation (16)

Journal of Information Systems Engineering and Management
2025, 10(47s)
e-ISSN: 2468-4376
https://www.jisem-journal.com/

Research Article

$$V_2 = V_{20} + \frac{1}{C_2}\int_0^T (I_{PV,out} + I_{BESS} + I_{grid,out} - I_{charging})dt \qquad (16)$$

The V_{20} is the initial bus voltage of the solar PV MPPT subsystem, C_2 is the DC MG capacitor value. Thesolar P.V. panel MPPT subsystem output current at time t is $I_{PV,out}$, BESS charging and discharging current is I_{BESS} (or I_2) and the final grid current output is $I_{grid,out}$. The BESS charging current is given by the equation (17)

$$I_{charging} = \frac{P_{charging}}{V_2 \eta_{DC-DC1}} \qquad (17)$$

In this, the BESS charging current is determined by the real power flow at the charging terminal through inductance L1. the DC MG voltage is V2 and the efficiency of the dc to dc bidirectional chopper ηDC-DC1. This efficiency depends on the load chopper converter also. The M.G. current output Igrid,out is given in equation (18) in terms of the M.G. real power Pgrid, MG voltage V2, and grid boost voltage conversion efficiency ηDC-DC2.

$$I_{grd,out} = \frac{P_{grid}}{V_2}\eta_{DC-DC2} \qquad (18)$$

The BESS current flow into the M.G. is represented in terms of battery voltage E, the current through the battery cell IBESS with bidirectional dc to dc converter efficiency ηDC-DC3 is shown in equation (19)

$$I_{BESS,out} = \frac{EI_{BESS}}{V_2}\eta_{DC-DC3} \qquad (19)$$

The load voltage V_{load} or V3 is given by the buck chopper switching duty cycle d3 is provided by the equation (20).

$$V_{load} = V_2 \frac{1}{1-d3} \qquad (20)$$

M.G. terminal current img gives the dynamic dc link voltage (Vdc) through the diode D2 and the bidirectional buck-boost converter with switching duty-cycle d2 is given by equation (21). The constant a= 1 represents boost and a=-1 for buck operation. So, buck and boost operation controlled by the duty cycle d2 and grid currents.

$$\frac{dV_{dc}}{dt} = a(-\frac{i_{mg}}{C_2} + \frac{d_2 i_2}{C_2}) \qquad (21)$$

The bidirectional buck-boost converter inductor dynamic current flow iL2 is represented using the battery voltage E and M.G. voltage V2 is given by the equation (22).

$$\frac{di_{L2}}{dt} = a(\frac{E}{L_2} - d_2\frac{V_2}{L_2}) \qquad (22)$$

The vectorial controlled bidirectional buck-boost converter inductor current represented in terms of M.G. capacitor C2 in terms of transfer function form with the Laplace parameter 's' is given by equation (23)

$$\frac{\bar{i}_{L2}}{\bar{d}_2} = \frac{-C_2V_2s - d_2 i_{L2}}{C_2L_2s^2 + d_2^2} \qquad (23)$$

The M.G. terminal voltage-controlled V2 is done using a current-controlled tuned proportional-integral (P.I.)

Journal of Information Systems Engineering and Management
2025, 10(47s)
e-ISSN: 2468-4376
https://www.jisem-journal.com/

Research Article

controller is given by the equation (24). Here, the input inductor boost converter subsystem current reference ($\bar{i}_{L1}^{*}$) and actual boost converter current ($\bar{i}_{L1}$). The objective of the current P.I. controller is maintaining zero or very minimum value between the reference and the actual current value, and ideally, zero is its value.

$$\bar{V}_2 = (\bar{i}_{L1}^{*} - \bar{i}_{L1})(K_{pi} + \frac{1}{K_{ii}s}) \qquad (24)$$

The final terminal voltage V2 and the input solar P.V. current (iL1)are written in the transfer function model with current tuned P.I. controller and boost converter duty cycle d1 is given by the transfer function equation (25)

$$\frac{\bar{V}_2}{\bar{i}_{L1}^{*}} = \frac{-K_{pi}K_{ii}d_1V_2s - d_1V_2}{C_2s^3 - C_2V_2K_{pi}K_{ii}s^2 + (d_1^2K_{ii} - C_2V_2)s} \qquad (25)$$

Block Diagram Representation of Solar P.V. System based dc M.G.

The dc M.G. consisting of a solar P.V. cell system with closed-loop controller representation is shown in Fig.2. The current tuned P.I. controller block diagram is GPI(s), offset switching frequency (Gsw(s)), solar P.V. panel system connected to a dc M.G. is G.P.V. (s) and dc voltage gain function is given by Av(s). The current P.I. controller is given by the equation (26) with 's' as the Laplace parameter, current proportionality (Kpi), and the current integral constant (Kii).

$$G_{PI}(s) = K_{pi} + \frac{K_{ii}}{s} \qquad (26)$$

The offset switching block (GSW(s)) is a relay block that operates based on the reference (V_2^{*}), and actual M.G. voltage (V_2) is shown in equation (27)

$$G_{SW}(s) = \begin{cases} 1 & V_2 > V_2^{*} \\ 0 & V_2 < V_2^{*} \end{cases} \qquad (27)$$

The solar P.V. panel transfer function is considered to be a standard 2nd order function with natural undamped frequency (ω_n), and damping ratio (ξ) is given by the equation (28)

$$G_{PV}(s) = \frac{\omega_n^2}{s^2 + 2\xi\omega_n s + \omega_n^2} \qquad (28)$$

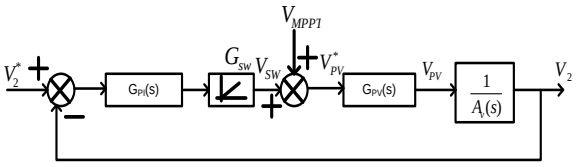

Figure 2. Solar P.V. microgrid block diagram representation

The dc-dc M.G. voltage gain in BESS switching duty cycle d2 and solar P.V. panel inductor L1and MG capacitor C2 is given by the equation (29)

$$A_v(s) = \frac{1 - d_2}{L_1C_2s^2 + \frac{L_1}{R_1}s + (1 - d_2)^2} \qquad (29)$$

The MG terminal voltage (V_2) with initial voltage v_{20}, mppt voltage (V_{mppt}), output limited transfer function ($G_{olimit}(s)$) and MPPT output transfer function (G_{omppt}) is given by the transfer function equation (30)

$$V_2 = G_{olimit}(s)V_{20} - G_{omppt}V_{mppt} \qquad (30)$$

Journal of Information Systems Engineering and Management
2025, 10(47s)
e-ISSN: 2468-4376
https://www.jisem-journal.com/

Research Article

The internal transfer functions for the equation (30) are defined and shown in the equations from (31) to (33) as

$$G_{olimit}(s) = \frac{G_{PI}(s)G_{SW}(s)G_{PV}(s)}{G_{PI}(s)G_{SW}(s)G_{PV}(s) - A_V(s)} \quad (31)$$

$$G_{ompp t}(s) = \frac{G_{SW}(s)}{G_{PI}(s)G_{SW}(s)G_{PV}(s) - A_V(s)} \quad (32)$$

$$G_{vmppt}(s) = \frac{\Delta V_2}{\Delta V_{mppt}} = -\frac{G_{PI}(s)}{G_{PI}(s)G_{PV}(s) - A_V(s)} \quad (33)$$

The change or error in the M.G. terminal voltage is given by the difference between reference and actual M.G. voltage, as shown by equation (34). Here, the error in the M.G. terminal voltage to zero is the objective.

$$\Delta V_2 = V_2^* - V_2 = \underset{s\to 0}{lt}\, s\Delta V_2 = 0 \quad (34)$$

The final output microgrid voltage is represented in the form of a transfer function (Gov(s)) in terms of a controller transfer function, solar P.V. panel transfer function, and dc-dc M.G. voltage gain as depicted by equation (35)

$$G_{ov}(s) = G_{PI}(s)G_{PV}(s)\frac{1}{A_V(s)} \quad (35)$$

The ratio of integral to proportional gain constants with a frequency of operation from 5 to 150 Hz is given by (36)

$$\frac{K_{ii}}{K_{pi}} = 2\pi * 100 \quad (36)$$

The final output voltage transfer function is controlled to 1 p.u.,(per unit) value as equation (37)

$$\left|G_{ov}(s)\right|_{s=-j20\pi} = 1 \quad (38)$$

From the equation (35), the open loop output microgrid voltage transfer function based Bode plot and Root-Locus plots are shown for different integral constants are shown in Fig. 3. and Fig.4. bwith plot parameters are shown in table 1. With increase in the K_{ii}, the phase margin is moving away from -180 degrees and gain margin is decreasing considerably, thereby stability margin is decreasing. the normal values of K_{pp} and K_{ii} are 1.22e-3 and 0.77.

Journal of Information Systems Engineering and Management
2025, 10(47s)
e-ISSN: 2468-4376
https://www.jisem-journal.com/

Research Article

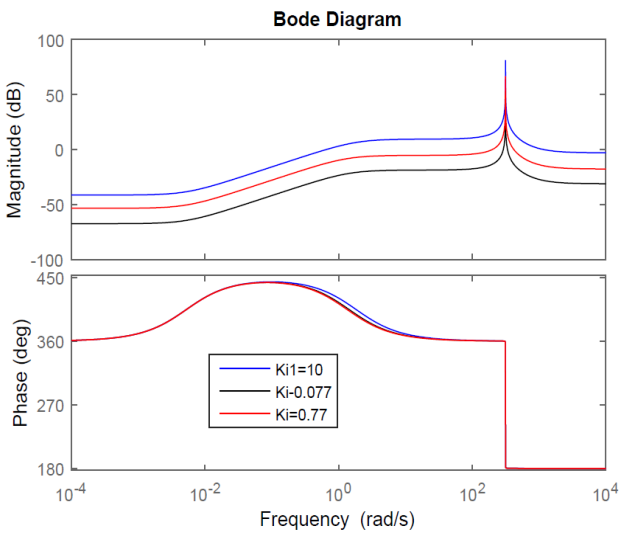

Figure 3. Bode Plot for Gov(s)

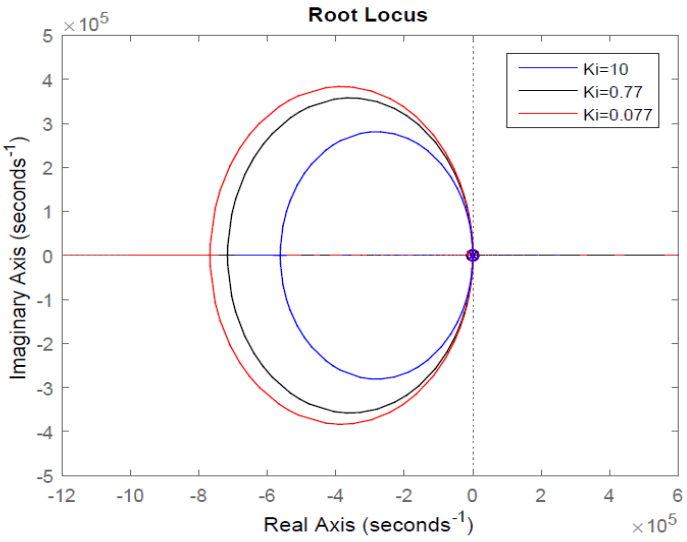

Figure 4. Root-Locus Plot for $G_{ov}(s)$

TABLE 1

Table 1. The frequency domain analysis parameters for different k_{ii} values

Parameters	Gain Margin	Phase Margin	PM Frequency	Delay Margin	DM Frequency	Stable
Ki=10	1.4084	-110.2359	0.6537	6.6688	0.6537	1
Ki=0.77	35.8508	-179.8441	291.3206	0.0108	291.3206	1
Ki=0.077	7.6823	-179.6415	199.9663	0.0157	199.9663	1

TWO AREA-BASED SOLAR PV DC MICROGRID TESTBED SYSTEM

A two-area testbed system interconnected by a shared transmission line network is shown in Fig.5. Each area consists of a small microgrid (M.G.) generation system, a BESS, and a solar-PV panel with dc-dc MPPT system tied to a common dc micro-grid with internal loading as shown in Fig.6.

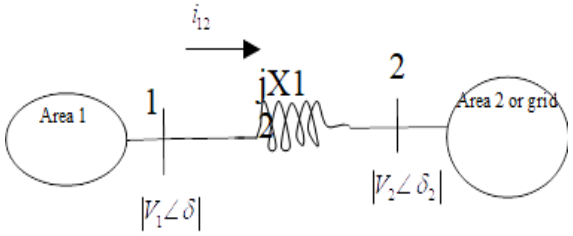

Figure 5. Two area system under study with FACTS device

Journal of Information Systems Engineering and Management
2025, 10(47s)
e-ISSN: 2468-4376
https://www.jisem-journal.com/

Research Article

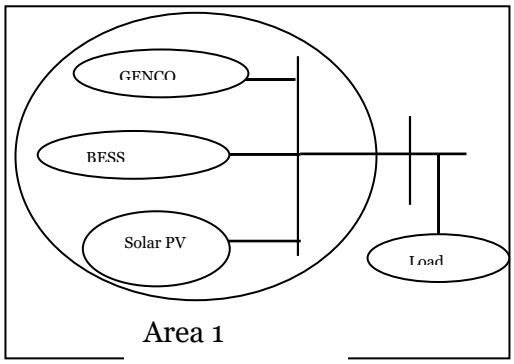

Figure 6. One area source, load schematic

The solar P.V. panel system with an inverter unit simplified block diagram is shown in Fig.5. There will be a source side inductor for current smoothening and then a switch in parallel for chopping or regulating dc voltage application to a constant voltage irrespective of irradiance. Then, capacitors supply constant voltage to the inverter switches even with a large load or grid disturbances. The filter bank contains L.C.L. elements to improve the voltage and current waveforms to the grid requirements. The (IV) current-voltage and (P.V.) power-voltage characteristics of the solar panel at different irradiance values are shown in Fig. 7. and Fig. 8.

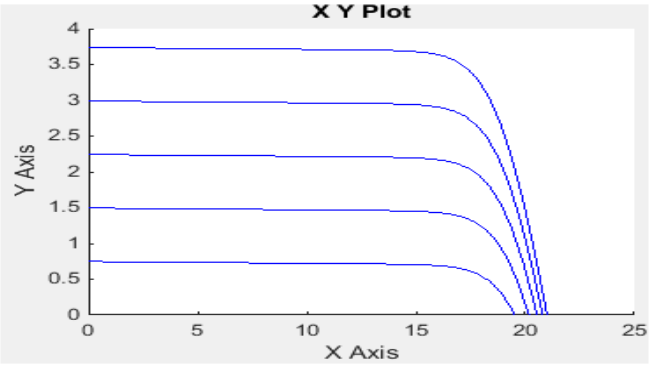

Figure 7. IV- Characteristics

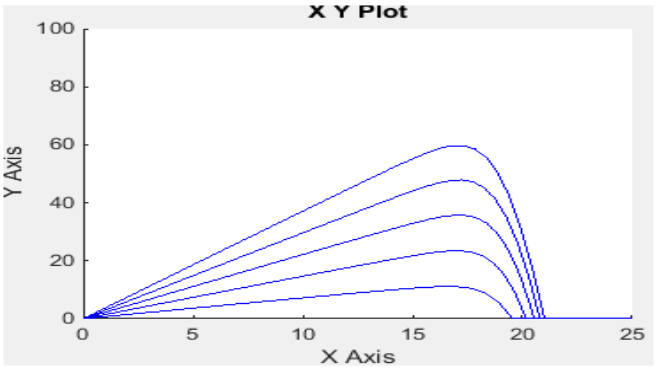

Figure 8. PV- Characteristics

The values of the DC MG solar PV BESS panel system parameters are shown in the Appendix at the end of the paper Conclusion section. The solar panel current-voltage (IV) and power-voltage (P.V.) characteristics at different irradiance values simulation outputs is shown in Fig.7. and Fig.8.

Modeling of Bess for Solar PV Grid-Connected System For Real Power Flow Sharing

The grid voltage is supposed to be 230V, and the battery converter voltage set at 1.2 times the voltage, which is 276V. If for a nominal lithium-ion battery rating of 9V, the number of series battery cells required is (270/9) 31number. If an Ampere-hour of the battery set to 100, and the power rating for compensation for the solar PV-load system is assumed to be 300KWh, the desired Ah is (300K/276)= 1087Ah and hence requires (1087/100)=11 cells in parallel. For a voltage source of 276 V the Li-ion battery modellingwith the equivalent capacitance Cb is given as [35]. To analyse the battery energy storage with the parallel combination of capacitance (Cb) and resistance (Rb) in series with internal resistance (Rin) is done using Thevenin's model [35].

Solar PV Panel Closed Loop Control for Maximum Real Power Extraction

The maximum power point tracking (MPPT) technique is generally adopted extractmaximum power from the PV cell. The solar PV panel performance will be improved and voltage profile can be maintained at desirable valuecan be done based on the MPPT technique adopted. There are numerous MPPT techniques available in the literature

Journal of Information Systems Engineering and Management
2025, 10(47s)
e-ISSN: 2468-4376
https://www.jisem-journal.com/

Research Article

like Hill climbing etc as discussed in the Section 1. Generally closed loop control schemes are used to track the MPPTfor available temperature and irradiance at that erection point. The basic control scheme of the solar PV cell with closed loop transfer function scheme is shown in Fig.9.

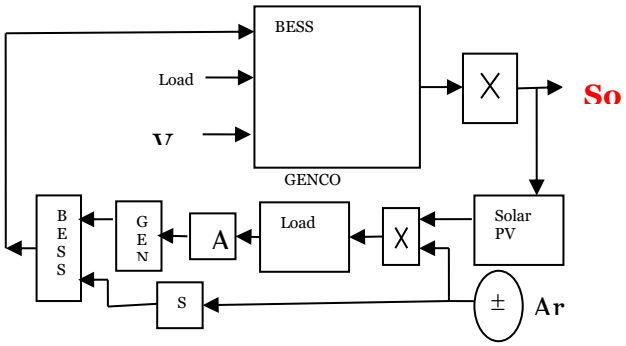

Figure 9. Solar PV closed loop system

The solar PV cell will produce anode voltage (Va)for a natural solar irradiance (Irrad) and ambient temperature (Temp) in degrees at the erection point. The output from solar PV cell is a variable current (I_pv). When this anode voltage is multiplied with the cell current, output power obtained is (P_pv). A first order transfer function model will describe the PV cell power depending on the power constants A and K1 as constants. The output from this A, K1 block transfer function is the reference current. The nominal frequency can be (50 or 60Hz) for a 1 volt dc reference per unit (p.u.) voltage (V_ref). The p.u. voltage is multiplied with this transfer function derived current to extract the reference power value, which is in general the characteristic power of solar PV cell. This power is made optimal so as to achieve the maximum power from the solar cell. To achieve this,one more first order transfer function block with constantsB and K2. These constants based transfer function is multiplied with a current gain constant C to obtain maximum current extraction value from solar cell.

An integrator in Laplace coefficient S is used to get the area under the curve and to observe its utmost value from the orientation curve. This highestpeak voltage endas added with reference sinusoidal input voltage and meant to the solar PV cell inputanode voltage. This basic mechanism assists in two fold. First advantage is to obtain maximum power point (MPP) in the P-V curve and to build it to become stable at this point. Second benefit is to formulate the solar PV cell voltage to maintainunvarying for small variations in the irradiance and temperature. The results for proposed control circuit design is discussed in the next section. The values taken in this paper are A=5, B=5.5, C=13.8, D=1/25,K1=0.5, and K2=0.5, for a single unit PV panel.

SOLAR P.V WITH MPPT DESIGN WITH METAHEURISTIC-PID (MPID CONTROL SCHEME)

This section discusses MATLAB/Simulink-based design of proportional integral and derivative (PID) Control Scheme. The error in the dc M.G.voltage is the input, and the reference current is the output of the PID controller in this paper. The adaptive P.I.D. Controller with P, I, and D tuning mechanism with initial values adjusted to Kpo, Kdo, and Kio are shown in Fig. 10. These sum and initial value blocks are multiplied with respective proportional, derivative and integral weights to get output reference parameter (u). In this paper, the output (u) is the current reference value. The sub-block of sumKp, sumKd, and sumKi consists of memory block and is shown in Fig.11.

Journal of Information Systems Engineering and Management
2025, 10(47s)
e-ISSN: 2468-4376
https://www.jisem-journal.com/

Research Article

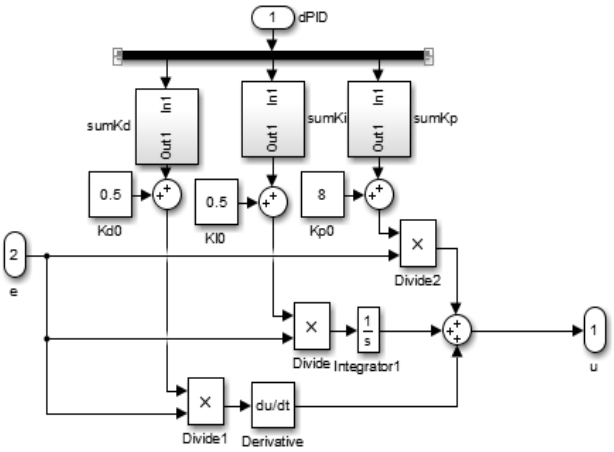

Figure 10. Output sub-block diagram to get output

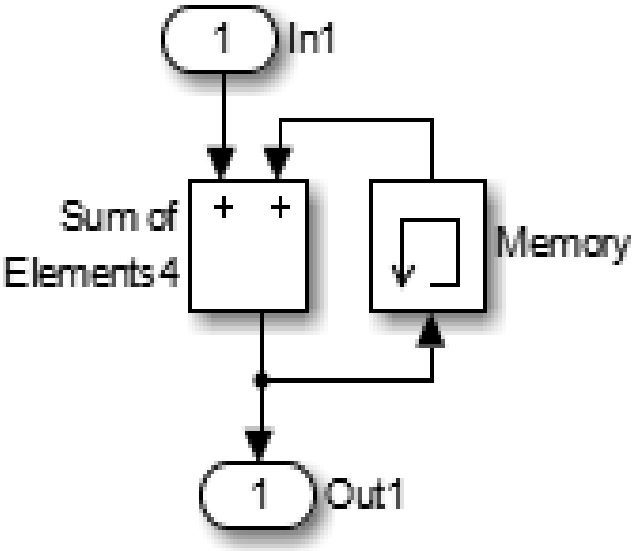

Figure 11. PID error-gain sub-block

Journal of Information Systems Engineering and Management
2025, 10(47s)
e-ISSN: 2468-4376
https://www.jisem-journal.com/

Research Article

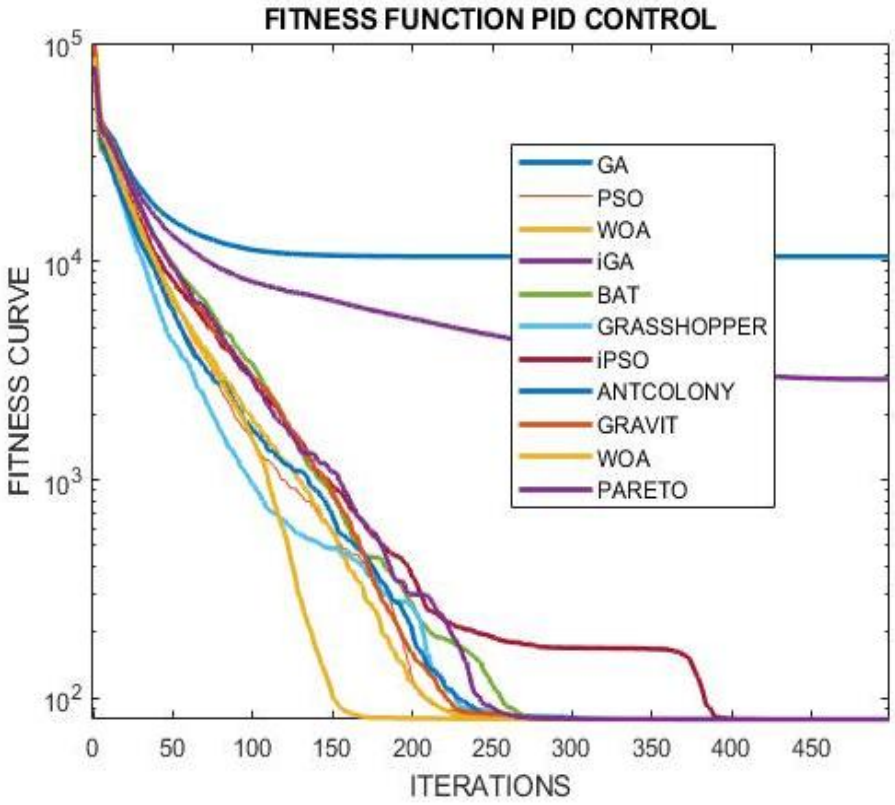

Figure 12. Fitness curve optimization graphs using various metaheuristic techniques

The different and most famous metaheuristic techniques like genetic algorithm (GA), particle swarm optimization (PSO), BAT, GWO, improved GA, improved PSO, grasshopper, Ant-Bee Colony, Gravity search, WOA and Pareto search are used for PID tuning and the fitness curve with 500 iterations count is observed as shown in Fig. 12. It is found that GWO and WOA are having very quick fitness curve capability, improved dynamic response, better stability enhancement characteristics among all these metaheuristic algorithms. Hence, we considered to show the GWO and WAO algorithms for oscillations damping and stability improvement in a dc microgrid with solar BESS power network in the next section analyzing about the results. The different pseudo-codes for few algorithms are discussed very briefly and complete details will be available in the respective references. This paper used these techniques for the proposed network with PID controller performance enhancement.

The multi-objective pseudo code for solar PV MPPT using Gravitational Search Algorithm (GSA) [36 and 37] is shown in algorithm 1. While the real coded binary ant bee colony algorithm for a generalized system with islanded microgrid [38] is shown in algorithm 2.

Algorithm 1:
Gravitational Search Algorithm (GSA)

Journal of Information Systems Engineering and Management
2025, 10(47s)
e-ISSN: 2468-4376
https://www.jisem-journal.com/

Research Article

```
Begin
    initialize population and evaluate generation
    evaluate fitness of agents
while
        test for population, mutation until not met;
        evaluate different directions of total force;
        calculate velocity and acceleration;
        repeat while loop
end
end
```

Algorithm 2:
Real Coded Ant Bee Colony Algorithm (RCABC)

```
Begin
    initialize population
    evaluate fitness
while
        apply greedy selection process;
        for every unemployed bee;
            look for new population;
check for fitness
            apply and update for greedy selection process
        until (best solution achieved)
end
end
```

Journal of Information Systems Engineering and Management
2025, 10(47s)
e-ISSN: 2468-4376
https://www.jisem-journal.com/

Research Article

Algorithm 3:
Strength Pareto Evaluation Algorithm (SPEA)

Begin
initialize population
evaluate solutions
create empty external set
test for fitness in population and
test further for external set
while
update external set;
repeat till number of non-dominated solutions are higher than the specified size of external set;
or maximum number of generations are achieved;
making pool updated with binary tournament
solution with replacement on updated external set
check for best solution
end
end

Thesolar photovoltaic MPPT and stability enhancement using WOA and GWO algorithms are discussed in [40 and 41] and their pseudo-code algorithms are discussed briefly in algorithms4 and 5.

Algorithm 4:
Whale Optimization Algorithm (WOA)

Begin
initialize population of whales randomly
create fitness for search and grading of all the whales
test for fitness in population and
test further for best search agent (X)
while
Calculate value of a and other parameters
for h< 0.5 and then for h>0.5
different $|A|$ values, calculate X
each search agent
repeat till all agents, and positions are checked;
update and repeat for all the grading agents
or maximum number of populations are achieved;
solution with replacement on updated agent solution
check for best solution
repeat all these steps till all the iterations are checked
end
end

Journal of Information Systems Engineering and Management
2025, 10(47s)
e-ISSN: 2468-4376
https://www.jisem-journal.com/

Research Article

Algorithm 5: **Grey Wolf Optimization Algorithm (GWO)**
Begin
initialize population of grey wolves, a, A and C
evaluate solutions
create fitness for search and grading of agents
test for fitness in population and
test further for first, second and third best solutions
while
for each search agent
update search agent position;
repeat till all agents, and positions are checked;
update and repeat for all the grading agents
or maximum number of populations are achieved;
solution with replacement on updated agent solution
check for best solution
repeat all these steps till all the iterations are checked
end
end

RESULT ANALYSIS

The solar PV BESS system connected to a dc M.G. with voltage control action using GWO and WAO and without controller response is shown in Fig. 13. to Fig. 23.. The M.G. is started suddenly at 1 second of simulation time, and different parameters' response is analyzed. Based on Fig. 13, the solar P.V.increases output voltage without a controller with time and is said to be unstable when black-started immediately. With WAO, the solar P.V. output has a peak value of 1.065 p.u.,(perunit)and reaches reference 1.02 value at 3 seconds (s) without oscillations. With GWO, the voltage at the start is 0.99 and also settles at 3s. It can be observed that instead of voltage peak (rise) with WAO, the dip, which is a better feature for GWO proposed. The oscillations are damped effectively, and improved overall stability with WAO and GWOobserved a better response with GWO.

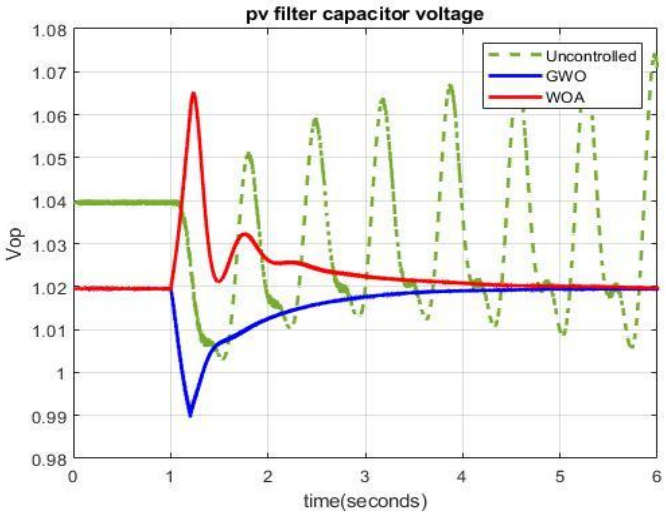

Figure 13. Solar PV output voltage

Journal of Information Systems Engineering and Management
2025, 10(47s)
e-ISSN: 2468-4376
https://www.jisem-journal.com/

Research Article

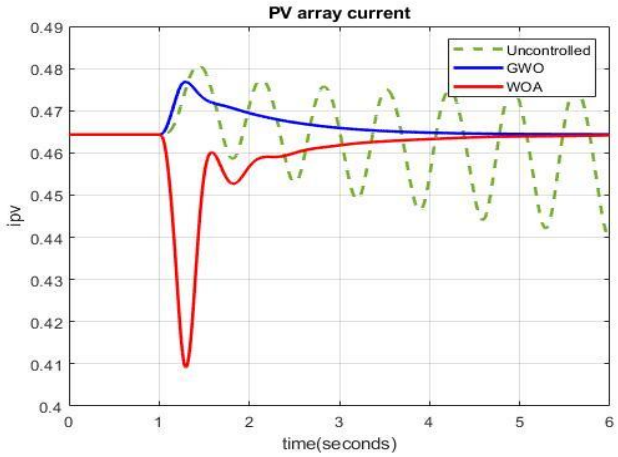

Figure 14. Solar PV current after MPPT

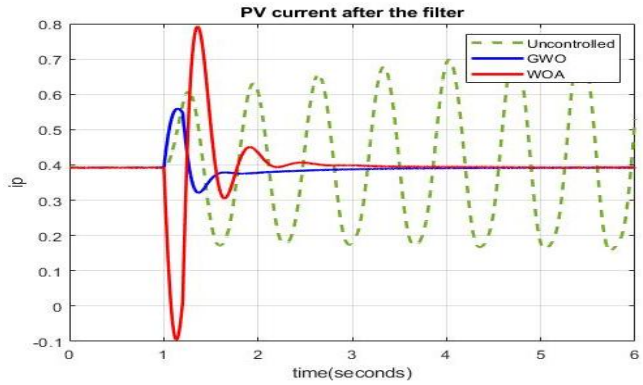

Figure 15. Solar PV current after filter

The solar P.V. current output after MPPT without a controller, with WAO and GWO, is shown in Fig. 14. The solar P.V. current is unstable without a controller, is having starting impulse to a value of 0.41 pu, and reached its reference value of 0.465 p.u., with WAO and settled at 3s. With the proposed GWO, the current rises to 0.476 p.u., and settles at the same period of 3s. The current surge value is smaller with GWO compared to the WAO value. The solar P.V. panel output current after the inductor filter bank and at the point of M.G. connection without a controller, with WAO and GWO, is shown in Fig. 15. The solar current after the filter bank is having a sustainable operation without a controller with oscillations from 0.65 to 0.2 p.u., range. With FPID, the current surge at 1s black-start has a large spike varying between -0.1 p.u.,and 0.8 p.u.,and settles at 3s and has two considerable oscillations. The same current with GWO, the current starting surge is 0.55 p.u., and settles at 1.5s to the reference value of 0.4 p.u., depicts better settling time, lower peak-overshoot, quicker and smoother response.

The solar P.V. current before the filter without a controller, with WAO and GWO, is shown in Fig. 16. The current is oscillatory when using the controller. With FPID, the current surges starting are 0 to 0.8 p.u., and settle at 2.5s with three damped oscillations and settled at 0.4 p.u., reference value. The same current has a peak of 0.58 p.u., at 1s, and resolves to 0. p.u., at 1.5s with effective damping.

Journal of Information Systems Engineering and Management
2025, 10(47s)
e-ISSN: 2468-4376
https://www.jisem-journal.com/

Research Article

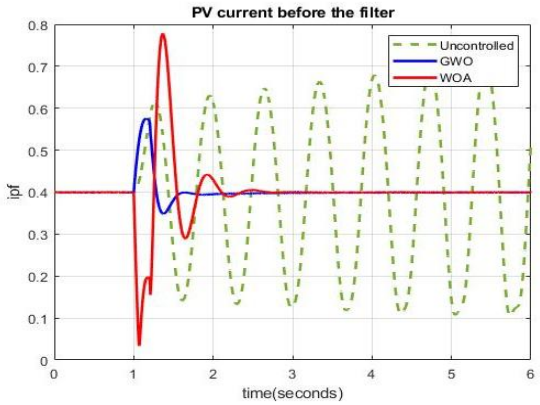

Figure 16. Solar PV current before filter

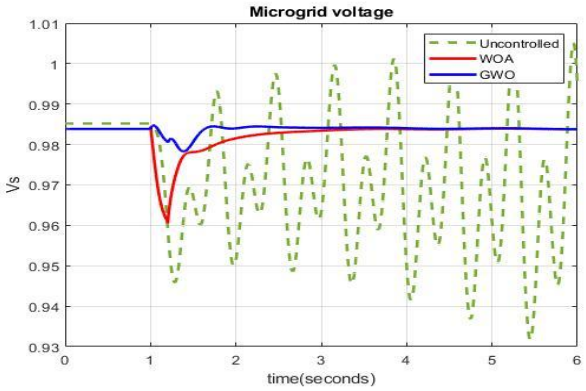

Figure 17. MG injected voltage

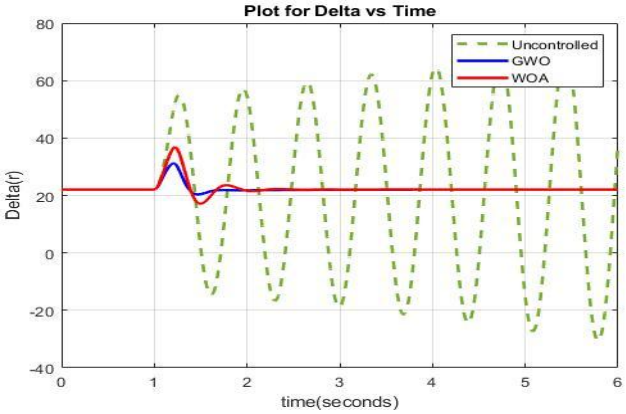

Figure 18. SG power angle (delta)

The voltage at the M.G. terminal (V2) without a controller, with FPID, and with GWO is shown in Fig. 17. The M.G. voltage is unstable when the controller is not used, and the range of oscillations is from 1 to 0.93 p.u.,and increasing with time. The WAO based M.G. voltage has a voltage dipped to 0.98 p.u., when the solar PV system is started at 1 p.u., and settles at 3s to 0.982 p.u., reference value. The M.G. voltage with GWO, voltage dipped to 0.98 p.u., and settles to 0.98 p.u., reference voltage quickly at 1.5s smoothly and without oscillations. The S.G. load angle (delta) plot with time in Fig. 18. The load angle is unstable without any controller and oscillates between 60 and -40 degrees, increasing exponentially and cosine with time. The WAO and GWO based load angle in degrees increased to 38 and 30 degrees and settled at 2s and 1.5s, respectively, and settled to 20 degrees after that.

Journal of Information Systems Engineering and Management
2025, 10(47s)
e-ISSN: 2468-4376
https://www.jisem-journal.com/

Research Article

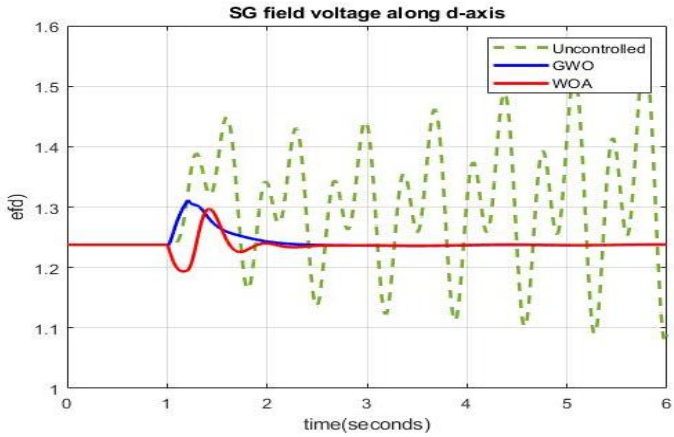

Figure 19. SG d-axis voltage

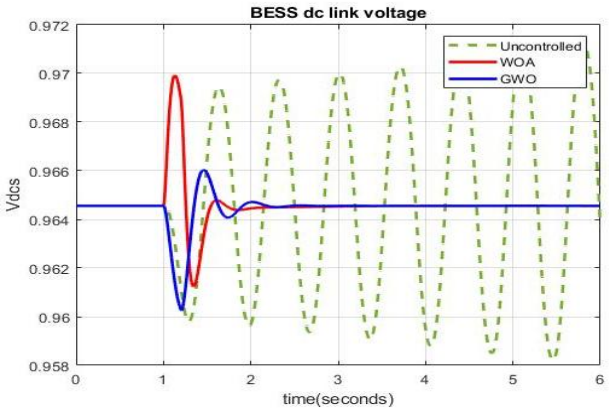

Figure 20. BESS dc link voltage

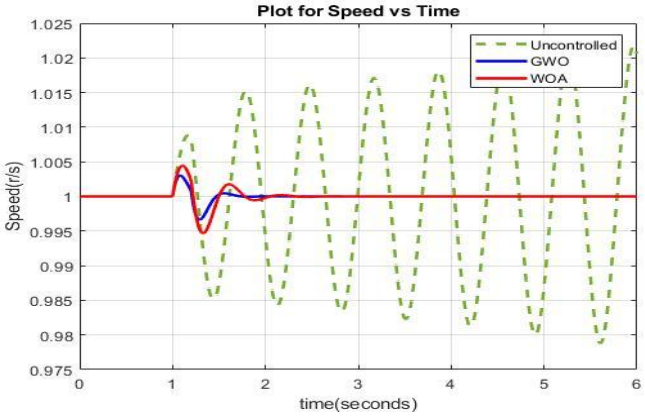

Figure 21. SG rotor speed

The d-axis voltage of the S.G. is shown in Fig. 19. Without a controller, voltage is unstable and increasing oscillatory with a range of 1.5 to 1.1 p.u. With the FPID, this d-axis S.G. voltage has two oscillations in the range of 1.3 to 1.2 p.u. and settles at 2.5s to 1.25 p.u.. The d-axis voltage with the GWO controller rises to 1.3 p.u.,with a single oscillation and settles at 2.5s. The BESS terminal voltage without a controller, with WAO and GWO, is shown in Fig. 20. The battery chopper voltage rises to 0.97 p.u., then to 0.96 p.u., and then settles to 0.965 p.u.,at 2.5s, the same voltage with GWO reached 0.96 and then settled at 2s at 0.965 p.u. The GWO is not producing overshoot and results in a smoother and quicker response than the WAO controller.

Journal of Information Systems Engineering and Management
2025, 10(47s)
e-ISSN: 2468-4376
https://www.jisem-journal.com/

Research Article

The S.G. rotor speed without any controller, with WAO and with GWO is shown in Fig. 21. The pace is oscillatory and unstable when not using the controller. The rotor speed changed from 1.005 to 0.995 p.u.,and settles at 2s, while with GWO, the rotor speed changed from 1.003 to 0.998 p.u., and drops at 1.5s to 1 p.u., speed value.

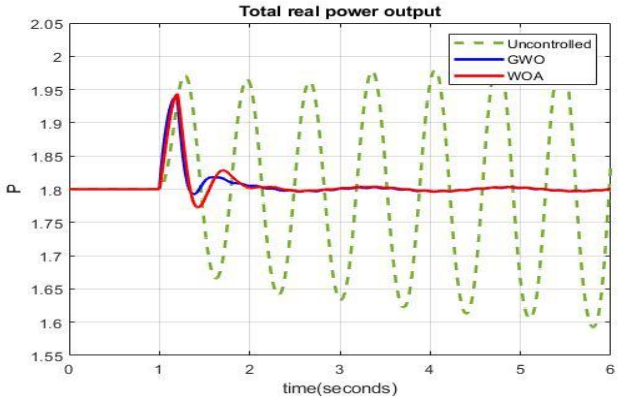

Figure 22. Injected real power

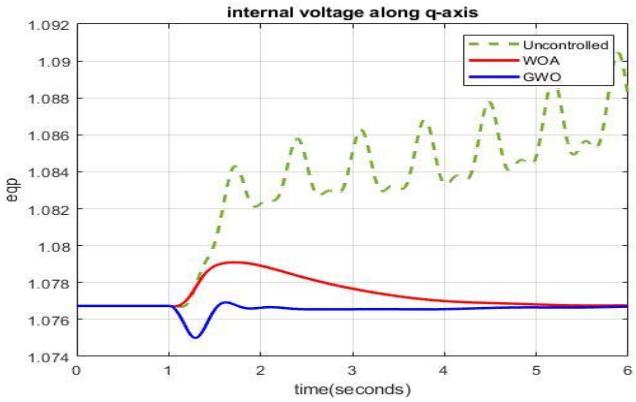

Figure 23. Internal voltage along q-axis supplied to the M.G.

The real power injected to the dc M.G. by the solar PV BESS system without a controller, FPID, andGWO controller is shown in Fig. 22 The real power is unstable and oscillatory when using no controller. With FPID, the real power increased to 1.95 and then to 1.78 p.u., then settles to 1.8 p.u. At 2.2s and with GWO, the real power injected rises to 1.93, then to 1.8 p.u., and pays at 1.6s earlier than WAO controller. The real power injected into the dc M.G. by a P.I. controller is 1.774940269747908 p.u, with FPID, 1.79214638652114 p.uGWO, 1.801264409755665 p.u. Hence, the active power injection is more with GWO compared to WAO and P.I.D.Controller. The elapsed time for the simulation took 25.569193 seconds to complete.

CONCLUSION

This paper presents the use of metaheuristic Proportional-Integral-Derivative (MPID) controllers, optimized using Whale Algorithm Optimization (WAO) and Grey Wolf Optimization (GWO), for enhanced power flow control and oscillation damping in a DC microgrid (MG) system. The performance of key components—including the synchronous generator (SG), solar photovoltaic (PV) cell, microgrid (MG), and battery energy storage system (BESS)—is analyzed during sudden start-up conditions. The BESS plays a critical role in supporting the PV system during periods of low or no solar generation, such as at night or under partial shading.

The results show that without any controller, system parameters become unstable, leading to significant oscillations. In this uncontrolled scenario, the system fails to maintain a constant grid voltage or rotor speed, and

exhibits sustained fluctuations in PV voltage, current, power angle (δ), rotor speed, and BESS terminal voltage. However, the application of WAO- and GWO-tuned PID controllers significantly improves the system's dynamic performance.

Among the two, the GWO-based controller demonstrates superior performance. It results in reduced peak overshoot, faster settling time, lower oscillations, and smoother system response compared to the WAO-based controller. Furthermore, the GWO controller exhibits faster computation time and better adaptability to various system parameters, making it less dependent on specific system conditions. Additionally, the GWO controller facilitates higher real power injection into the system. Therefore, the GWO-optimized PID controller proves to be more robust and effective than the WAO counterpart for regulating power flow and enhancing stability in DC microgrid applications.

Appendix

Inductances L_1, L_2 and L_3 are 5mH, capacitances C_1=200μF, C_2=2000μF and C_3=300μF, resistances R_1=14.4Ω, R_2=9Ω, R_E and R_L=1Ω, R_p=106Ω, I_{pv}=9A, a=0.767, β=0.05.

REFERENCES

[1] Tie, Siang Fui, and Chee Wei Tan. "A review of energy sources and energy management system in electric vehicles." Renewable and sustainable energy reviews 20 (2013): 82-102.
[2] Rauschenbach, Hans S. Solar cell array design handbook: the principles and technology of photovoltaic energy conversion. Springer Science & Business Media, 2012.
[3] Li, Quan, and Peter Wolfs. "A review of the single phase photovoltaic module integrated converter topologies with three different D.C. link configurations." IEEE Transactions on power electronics 23, no. 3 (2008): 1320-1333.
[4] Hafiz, Faeza, Anderson Rodrigo de Queiroz, and Iqbal Husain. "Multi-stage stochastic optimization for a PV-storage hybrid unit in a household." In 2017 IEEE Industry Applications Society Annual Meeting, pp. 1-7. IEEE, 2017.
[5] Gouda, Eid Abdelbaki, Ahmed Abd-Alaziz, and Magdi El-Saadawi. "Design modeling, and control of multi-stage SMES integrated with P.V. system." Journal of Energy Storage 29 (2020): 101399.
[6] Hu, Yihua, Wenping Cao, Bing Ji, Jikai Si, and Xiangping Chen. "New multi-stage D.C.–D.C. converters for grid-connected photovoltaic systems." Renewable energy 74 (2015): 247-254.
[7] Chaurasiya, Prem Kumar, Vilas Warudkar, and Siraj Ahmed. "Wind energy development and policy in India: A review." Energy Strategy Reviews 24 (2019): 342-357.
[8] https://www.worldenergy.org/data/resources/resource/solar/.
[9] El-Shahat, Adel, and Sharaf Sumaiya. "DC-microgrid system design, control, and analysis." Electronics 8, no. 2 (2019): 124.
[10] Nansur, Ainur Rofiq, Alfis Syah Laili Hermawan, and Farid Dwi Murdianto. "Constant voltage control using fuzzy logic controller (FLC) to overcome the unstable output voltage of MPPT in DC microgrid system." In 2018 International Electronics Symposium on Engineering Technology and Applications (IES-ETA), pp. 19-24. IEEE, 2018.
[11] Vasantharaj, Subramanian, Vairavasundaram Indragandhi, Vairavasundaram Subramaniyaswamy, Yuvaraja Teekaraman, Ramya Kuppusamy, and Srete Nikolovski. "Efficient Control of DC Microgrid with Hybrid PV—Fuel Cell and Energy Storage Systems." Energies 14, no. 11 (2021): 3234.
[12] Yan, Hein Wai, Glen G. Farivar, Neha Beniwal, Naga Brahmendra Yadav Gorla, Hossein Dehghani Tafti, Salvador Ceballos, Josep Pou, and Georgios Konstantinou. "Control strategy for effective battery utilization in a stand-alone dc microgrid with solar energy." In 2021 IEEE Energy Conversion Congress and Exposition (ECCE), pp. 1046-1051. IEEE, 2021.
[13] Satapathy, Manoranjan, Meher Preetam Korukonda, Amir Hussain, and Laxmidhar Behera. "A direct perturbation based sensor-free mppt with dc bus voltage control for a standalone dc microgrid." In 2019 IEEE PES Innovative Smart Grid Technologies Europe (ISGT-Europe), pp. 1-5. IEEE, 2019.
[14] Das, Saborni, Abhik Hazra, and Mousumi Basu. "Metaheuristic optimization based fault diagnosis strategy for solar photovoltaic systems under non-uniform irradiance." Renewable energy 118 (2018): 452-467.

[15] Pathak, Pawan Kumar, Anil Kumar Yadav, and P. A. Alvi. "A state-of-the-art review on shading mitigation techniques in solar photovoltaics via meta-heuristic approach." Neural Computing and Applications (2021): 1-39.
[16] Bodha, Kapil Deo, Vinod Kumar Yadav, and Vivekananda Mukherjee. "A novel quantum inspired hybrid metaheuristic for dispatch of power system including solar photovoltaic generation." Energy Sources, Part B: Economics, Planning, and Policy 16, no. 6 (2021): 558-583.
[17] Pillai, Dhanup S., and N. Rajasekar. "Metaheuristic algorithms for PV parameter identification: A comprehensive review with an application to threshold setting for fault detection in PV systems." Renewable and Sustainable Energy Reviews 82 (2018): 3503-3525.
[18] Mohamed, Mohamed A., Ahmed A. Zaki Diab, and Hegazy Rezk. "Partial shading mitigation of PV systems via different meta-heuristic techniques." Renewable energy 130 (2019): 1159-1175.
[19] Das, Monotosh, Maisanam Anil Kumar Singh, and Agnimitra Biswas. "Techno-economic optimization of an off-grid hybrid renewable energy system using metaheuristic optimization approaches–case of a radio transmitter station in India." Energy conversion and management 185 (2019): 339-352.
[20] Sun, Jiwei, Wei Lin, Mingguo Hong, and Kenneth A. Loparo. "Voltage Regulation of DC-microgrid with P.V. and Battery." IEEE Transactions on Smart Grid 11, no. 6 (2020): 4662-4675.
[21] Gu, Yunjie, Wuhua Li, and Xiangning He. "Passivity-based control of D.C. microgrid for self-disciplined stabilization." IEEE Transactions on Power Systems 30, no. 5 (2014): 2623-2632.
[22] Doshi, Karan, and V. S. K. V. Harish. "Analysis of a wind-PV battery hybrid renewable energy system for a dc microgrid." Materials Today: Proceedings (2020).
[23] Alam, Mohd, Kuldeep Kumar, Saket Verma, and Viresh Dutta. "Renewable sources based D.C. microgrid using hydrogen energy storage: Modelling and experimental analysis." Sustainable Energy Technologies and Assessments 42 (2020): 100840.
[24] Wang, Shuoqi, Languang Lu, Xuebing Han, Minggao Ouyang, and Xuning Feng. "Virtual-battery based droop control and energy storage system size optimization of a D.C. microgrid for electric vehicle fast charging station." Applied Energy 259 (2020): 114146.
[25] Han, Ying, Hanqing Yang, Qi Li, Weirong Chen, Firuz Zare, and Josep M. Guerrero. "Mode-triggered droop method for the decentralized energy management of an islanded hybrid P.V./hydrogen/battery D.C. microgrid." Energy 199 (2020): 117441.
[26] Matayoshi, Hidehito, Mitsunaga Kinjo, Shriram S. Rangarajan, Girish Ganesan Ramanathan, Ashraf M. Hemeida, and Tomonobu Senjyu. "Islanding operation scheme for D.C. microgrid utilizing pseudo Droop control of photovoltaic system." Energy for Sustainable Development 55 (2020): 95-104.
[27] Singh, Prashant, and J. S. Lather. "Dynamic current sharing, voltage and S.O.C. regulation for HESS based D.C. microgrid using CPISMC technique." Journal of Energy Storage 30 (2020): 101509.
[28] Singh, Prashant, and J. S. Lather. "Dynamic current sharing, voltage and S.O.C. regulation for HESS based D.C. microgrid using CPISMC technique." Journal of Energy Storage 30 (2020): 101509.
[29] Naik, Jyotirmayee, Snehamoy Dhar, and P. K. Dash. "Adaptive differential relay coordination for PV DC microgrid using a new kernel based time-frequency transform." International Journal of Electrical Power & Energy Systems 106 (2019): 56-67.
[30] Armghan, Hammad, Ming Yang, M. Q. Wang, Naghmash Ali, and Ammar Armghan. "Nonlinear integral backstepping based control of a D.C. microgrid with renewable generation and energy storage systems." International Journal of Electrical Power & Energy Systems 117 (2020): 105613.
[31] Nguyen, Duy-Long, and Hong-Hee Lee. "Fuzzy P.I.D. Controller for Adaptive Current Sharing of Energy Storage System in D.C. Microgrid." In International Conference on Intelligent Computing, pp. 213-223. Springer, Cham, 2020.
[32] Al-Sakkaf, Shehab, Mahmoud Kassas, Muhammad Khalid, and Mohammad A. Abido. "An energy management system for residential autonomous D.C. microgrid using optimized fuzzy logic controller considering economic dispatch." Energies 12, no. 8 (2019): 1457.
[33] Sun, Qian, Qiuye Sun, and Dehao Qin. "Adaptive fuzzy droop control for optimized power sharing in an islanded microgrid." Energies 12, no. 1 (2019): 45.
[34] Ananth, D., G. N. Kumar, D. Deepak Chowdary, and K. Appala Naidu. "Damping of Power System Oscillations and Control of Voltage Dip by Using STATCOM and UPFC." International Journal of Pure and

Research Article

Applied Mathematics 114, no. 10 (2017): 487-496.

[35] Gayathri, T., D. V. N. Ananth, GV Nagesh Kumar, and G. Sivanagaraju. "Enhancement in dynamic and LVRT behaviour of an EFOC controlled DFIG with integrated Battery Energy Storage System." In 2013 Annual IEEE India Conference (INDICON), pp. 1-6. IEEE, 2013.

[36] Pani, Alok Kumar, and Niranjan Nayak. "Forecasting solar irradiance with weather classification and chaotic gravitational search algorithm based wavelet kernel extreme learning machine." International Journal of Renewable Energy Research (IJRER) 9, no. 4 (2019): 1650-1659.

[37] Li, Ling-Ling, Guo-Qian Lin, Ming-Lang Tseng, Kimhua Tan, and Ming K. Lim. "A maximum power point tracking method for PV system with improved gravitational search algorithm." Applied Soft Computing 65 (2018): 333-348.

[38] Marzband, Mousa, Fatemeh Azarinejadian, Mehdi Savaghebi, and Josep M. Guerrero. "An optimal energy management system for islanded microgrids based on multiperiod artificial bee colony combined with Markov chain." IEEE Systems Journal 11, no. 3 (2015): 1712-1722.

[39] Basu, M. "Economic environmental dispatch of solar-wind-hydro-thermal power system." Renewable Energy Focus 30 (2019): 107-122.

[40] Xiong, Guojiang, Jing Zhang, Dongyuan Shi, and Yu He. "Parameter extraction of solar photovoltaic models using an improved whale optimization algorithm." Energy conversion and management 174 (2018): 388-405.

[41] Chawla, V., A. Chanda, and S. Angra. "Automatic guided vehicles fleet size optimization for flexible manufacturing system by grey wolf optimization algorithm." Management Science Letters 8, no. 2 (2018): 79-90.